DMD Fast Forward. Published on August 16, 2016 as DOI: 10.1124/dmd.116.070920
This article has not been copyedited and formatted. The final version may differ from this version.

A high dose of isoniazid disturbs endobiotic homeostasis in mouse liver

Feng Li, Pengcheng Wang, Ke Liu, Mariana G. Tarrago, Jie Lu, Eduardo N. Chini, and Xiaochao Ma

Department of Molecular and Cellular Biology, Alkek Center for Molecular Discovery, Baylor College of Medicine, Houston, TX (F.L.);

Center for Pharmacogenetics, Department of Pharmaceutical Sciences, School of Pharmacy, University of Pittsburgh, Pittsburgh, PA (P.W., K.L., J.L., X.M.)

Laboratory of Signal Transduction, Department of Anesthesiology and Kogod Center on Aging, Mayo Clinic College of Medicine, Rochester, MN (M.G.T., E.N.C.)

Running title: Acute effect of isoniazid on liver metabolome

Corresponding author: Xiaochao Ma, Ph.D., Center for Pharmacogenetics, Department of Pharmaceutical Sciences, School of Pharmacy, University of Pittsburgh, Pittsburgh, PA 15261. Tel. (412) 648-9448, E-mail: mxiaocha@pitt.edu

Number of Text Pages: 28

Number of Table: 0

Number of Figures: 8

Number of References: 55

Number of Words in the Abstract: 186

Number of Words in the Introduction: 730

Number of Words in the Discussion: 1500

Abbreviations: INH, isoniazid; TB, tuberculosis; NAD, nicotinamide adenine dinucleotide; PL, pyridoxal; PLP, pyridoxal phosphate; HFBA, heptafluorobutyric acid; UPLC-QTOFMS, ultraperformance liquid chromatography coupled to quadrupole time-of-flight mass spectrometry; PCA, principal component analysis; OPLS-DA, orthogonal partial least-squares discriminant analysis

Abstract

Overdose of isoniazid (INH), an anti-tuberculosis drug, can be life-threatening because of neurotoxicity. In clinical practice for management of INH overdose and acute toxicity, the potential of INH-induced hepatotoxicity is also considered. However, the biochemical basis of acute INH toxicity in the liver remains elusive. In the current study, we used an untargeted metabolomic approach to explore the acute effects of INH on endobiotic homeostasis in mouse liver. We found that overdose of INH resulted in accumulation of oleoyl-L-carnitine and linoleoyl-L-carnitinein the liver, indicating mitochondrial dysfunction. We also revealed the interactions between INH and fatty acyl-CoAs by identifying INH-fatty acid amides. In addition, we found that overdose of INH led to the accumulation of heme and oxidized nicotinamide adenine dinucleotide (NAD) in the liver. We also identified an INH and NAD adduct in the liver. In this adduct, the nicotinamide moiety in NAD was replaced by INH. Furthermore, we illustrated that overdose of INH depleted vitamin B6 in the liver and blocked vitamin B6-dependent cystathionine degradation. These data suggest that INH interacts with multiple biochemical pathways in the liver during acute poisoning caused by INH overdose.

Introduction

Tuberculosis (TB) is a public health problem (Orcau et al., 2011). In 2012, there were ~8.6 million incident cases of TB and ~1.3 million TB-associated deaths worldwide (WHO, 2013). Isoniazid, also known as isonicotinylhydrazide (INH), is a first-line drug for TB treatment and prevention. With the numbers of patients receiving INH remaining high, the number of acute poisoning cases is expected to be significant (Maw and Aitken, 2003). Accidental or intentional overdose of INH causes seizures, metabolic acidosis, coma and even death (Temmerman et al., 1999; Khoharo et al., 2009). In adults, the regular dose of INH is 300 mg/day (~5 mg/kg/day). Doses over 30 mg/kg/day often produce neurotoxicity and seizures. It has been estimated that INH is responsible for ~5% of all cases of seizures associated with drug intoxications (Olson et al., 1993). When ingested in amounts of 80 to 150 mg/kg/day or more, INH can rapidly be fatal because of acute neurotoxicity (Romero and Kuczler, 1998).

Besides neurotoxicity, INH poisoning causes hepatotoxicity. In a 2-year-old girl who accidentally received 2 g of INH, liver function tests were found to be abnormal (Caksen et al., 2003). In a 26-year-old man who ingested 8 g of INH, elevation of activities of serum aspartate aminotransferase, alanine aminotransferase, gamma-glutamyl transpeptidase, and prolonged prothrombin time were observed, suggesting the occurrence of INH-induced acute hepatitis (Tai et al., 1996). A higher dose of INH results in more significant liver injury, as shown by 20-fold increases of both serum aspartate aminotransferase and lactate dehydrogenase activities in a 21-year-old woman who ingested 12 g of INH (Bear et al., 1976). These clinical observations are supported by a preclinical study showing that a high dose of INH causes the accumulation of reactive oxygen species and reactive nitrogen species in mouse liver (Shuhendler et al., 2014).

Therefore, monitoring of liver functions and prothrombin time is recommended in clinical practice for management of INH poisoning (Romero and Kuczler, 1998).

Understanding the acute effects of INH on the liver will be helpful for management of INH-induced liver injury during INH poisoning (Tai et al., 1996; Romero and Kuczler, 1998; Temmerman et al., 1999). However, limited information is available in this regard (INCHEM, 2016). Metabolomics, a methodology for exploring metabolite profiles in biological matrices, has been considered a powerful tool for illustrating the biochemical basis of drug toxicity and disease (O'Connell and Watkins, 2010; Beyoglu and Idle, 2013). In the current study, we used a metabolomic approach to investigate endobiotic homeostasis in the liver of mice receiving a high dose of INH. We found that INH interacts with multiple biochemical pathways in the liver, including heme, fatty acids, oxidized nicotinamide adenine dinucleotide (NAD), vitamin B6, and cystathionine.

Materials and methods

Chemicals and reagents. INH, hemin, cystathionine, NAD, pyridoxal (PL), pyridoxal phosphate (PLP), heptafluorobutyric acid (HFBA), and porcine brain NAD-glycohydrolase (NADase) were purchased from Sigma-Aldrich (St. Louis, MO). Oleoyl-L-carnitine and linoleoyl-L-carnitine were purchased from INDOFINE Chemical Company (Hillsborough, NJ). Deuterium-labeled INH (d4-INH) was purchased from Toronto Research Chemicals (Toronto, ON, Canada). All solvents for metabolite analysis were of the highest grade commercially available.

Animals and treatments. Mouse is a commonly used model for the studies on INH (Metushi et al., 2012). In the current study, wild-type mice (FVB/NJ, male, 8-week-old) were treated orally with INH at 0, 50 or 200 mg/Kg. These doses were chosen according to the dosage conversion factor between humans and mice (Reagan-Shaw et al., 2008). Because the regular dose of INH is 5 mg/kg/day in humans (INCHEM, 2016), 50 mg/Kg INH in mice mimics the pharmacological dose in humans; and 200 mg/Kg INH in mice mimics the toxic dose in humans. We did not choose the doses over 200 mg/Kg, because the LD50 of INH (*po*) in mice is 176 mg/Kg (INCHEM, 2016). To explore the effect of INH on liver metabolome, the mice were sacrificed at 30 min after INH treatment. Moribund was not observed at this time point Blood andliver samples were collected for metabolomic analysis. Serum alanine transaminase (ALT) and aspartate transaminase (AST) were also analyzed. We chose 30 min for sample collection, because most mice will die between 45 and 90 min after the treatment of 200 mg/Kg INH. To determine the time-dependent effect of INH on vitamin B6 in the liver, the mice were sacrificed at 15 and 45 min after INH treatment. All procedures involving mouse care and handling were in accordance with study protocols approved by the Institutional Animal Care and Use Committee.

Sample preparation. Liver tissues were homogenized in water (100 mg liver in 300 µl of water). Subsequently, a 400 µl aliquot of ice-cold MeOH was added to 200 µl of the resulting mixture, followed by vortexing and centrifugation at 18,000 *g* for 20 min. The supernatant was transferred to a new Eppendoff tube for second centrifugation (18,000 *g* for 10 min). Each supernatant was transferred to an auto sampler vial, and 5.0 µl was injected into an ultra-

performance liquid chromatography coupled with quadrupole time-of-flight mass spectrometry (UPLC-QTOFMS) for metabolite analysis.

UPLC-QTOFMS analysis. The same approach has been used in our previous studies on the metabolism of atazanavir and tipranavir (Li et al., 2010; Li et al., 2011a). In brief, a 100 mm x 2.1 mm (Acquity 1.7 µm) UPLC BEH C-18 column (Waters, Milford, MA) was used for metabolite separation. The flow rate of the mobile phase was set as 0.3 ml/min. The gradient ranged from 2% to 98% acetonitrile containing 0.1% formic acid in the first 8.5 min, 98% acetonitrile for 8.5 to 18 min, then equilibration at 2% acetonitrile for 2 min. QTOFMS (Waters, Milford, MA) was operated in a positive mode with electrospray ionization. The source temperature and desolvation temperature were set at 120 °C and 350 °C, respectively. Nitrogen was used as the cone gas and desolvation gas. Argon was applied as the collision gas. QTOFMS was calibrated with sodium formate and monitored by the intermittent injection of lock mass leucine enkephalin in real time. The capillary voltage and cone voltage were set at 3.5 kV and 35 V, respectively. Screening and identification of major metabolites were performed by using MarkerLynx software (Waters, Milford, MA) based on accurate mass measurement (mass errors less than 10 ppm). Tandem mass spectrometry fragmentation was conducted with collision energy ramp ranging from 10 to 40 V.

Inhibitory effect of INH on NADase activity. The inhibitory effect of INH (0 - 10 mM) on NADase activity was performed according to a previous report (Escande et al., 2013). Briefly, NADase activity was measured using recombinant human CD38 and expressed as arbitrary fluorescent units per minute (AFU/min).

Formation of INH-NAD adduct in S9 fraction of mouse liver and NADase. The metabolite VII was proposed as an INH-NAD adduct. To verify the structure of INH-NAD adduct and determine the role of NADase in formation of this adduct, we incubated INH or d_4-INH with NAD in S9 fraction of mouse liver and porcine NADase, respectively. Briefly, the reactions were conducted in an incubation system containing liver S9 fractions or NADase, 2 mM INH or d4-INH, and 2 mM NAD at 37 °C for 2 h. The reactions were terminated by adding two-fold volume of ice-cold MeOH, followed by vortexing and centrifugation at 10,000 *g* for 10 min. The supernatant was analyzed by UPLC-QTOFMS.

Bioanalysis of pyridoxal (PL) and pyridoxal phosphate (PLP). PL is one of the three natural forms of vitamin B6, and the active form of vitamin B6 is PLP. PL and PLP were analyzed according to a published method with a slight modification (van der Ham et al., 2012). In brief, an aliquot of 100 µl of liver homogenate was mixed with 20 µl of trifluoroacetic acid, followed by vortexing and centrifugation at 15,000 *g* for 10 min. Two µl of the supernatant was injected into the UPLC-QTOFMS system for analysis of PL and PLP. An Acquity HSS T3 column (100 mm x 2.1 mm, 1.7 µm) was used for chromatographic separation. A 4-min gradient at flow rate of 0.4 mL/min was used with mobile phase A (0.65 M acetic acid with 0.01% HFBA in water) and mobile phase B (0.65 M acetic acid with 0.01% HFBA in acetonitrile). The QTOFMS was operated in positive mode.

Synthesis of INH-PL adduct. We expected the formation of an INH-PL adduct. To verify its structure, we synthesized this adduct. Briefly, 200 µl of PL (400 µM in H_2O) and 200 µl of INH

(400 µM) were added to an Eppendorf tube. The resulting mixture was placed on a shaker at 37 °C for 30 min. The final product was analyzed by UPLC-QTOFMS. HRMS (ESI) Calcd. for $C_{14}H_{15}N_4O_3$ $[M+H]^+$ 287.1144, found 287.1146.

Metabolomic analysis. An untargeted metabolomic approach was used in the current study. Briefly, mass chromatograms and spectra were acquired by MassLynx software in centroid format from *m/z* 50 to 1000. Following deconvolution by MarkerLynx software, a multivariate data matrix containing information on sample identity, ion identity (retention time and *m/z*), and ion abundance was produced through deisotoping, filtering, peak recognition, and integration. We excluded INH and known INH metabolites (Li et al., 2011b) from the data matrix to focus on endobiotics in the liver. Principal component analysis (PCA) and orthogonal projection to latent structures-discriminant analysis (OPLS-DA) were further conducted on Pareto-scaled data to explore INH-mediated changes in liver metabolome. We next focused on the endogenous metabolites that were significantly altered after INH treatment.

Statistics. All quantified data are expressed as mean ± standard error of the mean (SEM). Statistical analysis was conducted using ANOVA. A p value of < 0.05 was considered statistically significant.

Results and discussion

Metabolomics has revealed elevation of bile acids, carnitine and carnitine derivatives in the urine and bile of mice chronically treated with a pharmacological dose of INH (Cheng et al., 2013). In addition, disturbance of heme synthesis pathway has been found in pregnane X receptor-

humanized mice chronically co-treated with rifampicin and INH (Li et al., 2013). However, limited information is available for the acute effects of INH on endobiotic homeostasis in the liver. In the current study, an untargeted metabolomic approach was used to address this topic in mice. The PCA analysis revealed two clusters corresponding to the control and 200 mg/Kg INH-treated groups in a score plot (Figure 1A). The corresponding S-plot displays the ion contribution to the group separation (Figure 1B). The top ranking ions were identified as heme (I), oleoyl-L-carnitine and linoleoyl-L-carnitine (II and III), INH-fatty acid amides (IV and V), NAD (VI), INH-NAD adduct (VII), and cystathionine (VIII). The serum metabolites were also profiled using the same method. However, the biomarkers identified in the liver cannot be found in the serum of mice treated with INH (Supplemental Table 1 and Supplemental Figure 1). In addition, treatment with INH had no significant effect on serum ALT and AST activities (Supplemental Figure 2).

INH-mediated accumulation of heme (I) in the liver

Metabolite I was eluted at 6.03 min (Figure 2A). MS/MS of metabolite I revealed the major product ions at *m/z* 616, 557 and 498 (Figure 2B), which exactly matched to the fragments of heme. The structure of metabolite I was further confirmed by comparing the retention time and MSMS to the authentic standard of heme. The INH-mediated accumulation of heme in mouse liver is dose-dependent. Compared to the control group, the levels of heme elevated 4 and 10 folds in 50 and 200 mg/Kg groups, respectively (Figure 2C).

Heme is a functional component of a variety of critical cellular proteins and is involved in numerous physiological processes such as oxygen transport, signal transduction, and cell

differentiation and proliferation (Beri and Chandra, 1993; Ponka, 1999). However, an excessive amount of free heme can cause membrane lipid peroxidation and the formation of reactive oxygen species, which eventually lead to the impairment of lipid bilayers and organelles, such as nuclei and mitochondria (Ryter and Tyrrell, 2000). Therefore, a high level of free heme will result in oxidative stress and tissue damage (Wagener et al., 2001; Wagener et al., 2003). We found that the levels of free heme increased in mouse liver shortly after INH treatment, suggesting that heme may contribute in part to liver damage during INH acute poisoning.

Heme homeostasis is tightly controlled. The biosynthetic pathway of heme includes eight enzymatic reactions taking place partly in the mitochondria and partly in the cytoplasm, whereas heme degradation is mediated by heme oxygenase 1 (HO-1) (Tenhunen et al., 1968; Tenhunen et al., 1969). The possible mechanisms of INH-mediated heme accumulation include (1) induction of heme biosynthesis; and (2) inhibition of HO-1-mediated heme degradation. Because the levels of heme in the liver increased shortly after INH treatment, it is more likely that INH inhibits heme degradation rather than the induction of heme biosynthesis. Further studies are needed to determine the mechanism by which INH disturbs heme homeostasis during INH acute poisoning.

INH-mediated accumulation of oleoyl-L-carnitine (II) and linoleoyl-L-carnitine (III) in the liver

Metabolite II was eluted at 7.48 min (Figure 3A). The MS/MS of II produced the major ions at *m/z* 426, 367, 144, and 85 (Figure 3B). Metabolite III was eluted at 7.15 min (Figure 3A), with a molecule $[M+H]^+$ at *m/z* = 424Da. The major fragmental ions of III included *m/z* 365, 144, and

85 (Figure 3C). Both metabolites II and III were identified as acylcarnitines because of their typical MS fragments at 85 and 144. Their structures were further determined as oleoyl-L-carnitine and linoleoyl-L-carnitine, respectively, by comparing the retention time and MSMS to the authentic standards. The INH-mediated accumulation of oleoyl-L-carnitine and linoleoyl-L-carnitine was dose-dependent (Figure 3D).

Mitochondrial dysfunction is one of the major mechanisms of drug-induced hepatotoxicity (Labbe et al., 2008; Pessayre et al., 2010; Pessayre et al., 2012). Long-chain fatty acid acylcarnitines are intermediates in fatty acid β-oxidation that occurs in mitochondria. Therefore, accumulation of oleoyl-L-carnitine and linoleoyl-L-carnitine suggests mitochondrial dysfunction (Makowski et al., 2009; Sampey et al., 2012). Studies have found that overdose of acetaminophen, a well-known hepatotoxin targeting mitochondria, leads to acylcarnitine accumulation in mice (Chen et al., 2009; McGill et al., 2014). In the current study, we found that overdose of INH resulted in acylcarnitine accumulation in the liver, indicating that a high dose of INH causes mitochondrial dysfunction. This finding is supported by the fact that hydrazine, an INH metabolite, suppresses mitochondria complex II (Lee et al., 2013; Boelsterli and Lee, 2014).

Formation of INH-fatty acid amides (IV and V)

Metabolites IV and V were eluted at 8.85 and 8.31 min, respectively (Figure 4A). The molecular weight (MW) difference of metabolites IV and V is 2 Da, but both of them have the major fragments of INH at *m/z* 138 and 121 (Figure 4B and 4C), suggesting the conjugation with INH. We further proved that metabolites IV and V are amides formed through the interactions between

INH and fatty acids. With the increase of INH dosage, the formation of INH-fatty acid amides IV and V increased significantly (Figure 4D).

The possible mechanism for the formation of INH-fatty acid amides (IV and V) was proposed as follows: (1) fatty acyl-CoA synthetase catalyzes fatty acids to form fatty acyl-CoAs; and (2) INH attacks fatty acyl-CoAs to form amides (Figure 4E). The formation of fatty-acyl-CoAs is an important step in fatty acid β-oxidation. Therefore, the interaction between INH and fatty-acyl-CoAs would reduce fatty acid β-oxidation. Together with the INH-mediated accumulation of oleoyl-L-carnitine and linoleoyl-L-carnitine (Figure 3), our results suggest that overdose of INH suppresses fatty acid metabolism, which may explain in part the mechanism of INH-induced fatty liver in mice (Richards et al., 2004; Church et al., 2014).

INH-mediated NAD (VI) accumulation in the liver

Metabolite VI was eluted at 0.87 min and had a protonated molecule $[M+H]^+$ at *m/z* = 664 Da. The MS/MS of metabolite VI produced the major ions at *m/z* 542, 524, 428, 348, 232, and 136, which exactly matched to the fragments of NAD (Figure 5A). The structure of metabolite VI was further confirmed by comparing the retention time and MSMS to the authentic standard of NAD. The INH-mediated NAD accumulation in mouse liver is dose-dependent (Figure 5B).

NAD, a coenzyme in redox reactions, serves as an electron carrier in fatty acid β-oxidation, glycolysis, and the Krebs cycle (Pollak et al., 2007). In addition to redox reactions, NAD participates in post-translational modifications of proteins, including NAD-dependent deacetylation and mono- and poly-ADP-ribosylation (Dolle et al., 2013). NAD-dependent

deacetylation is a key mechanism to control the activities of many mitochondrial enzymes that are involved in the Krebs cycle, fatty acid metabolism, antioxidant response, oxidative phosphorylation, and amino acid catabolism (Dolle et al., 2013; Nikiforov et al., 2015). Therefore, INH-mediated elevation of NAD in the liver may disrupt hepatic energy metabolism.

NAD is synthesized either in a *de novo* pathway from amino acids or in salvage pathways by recycling preformed components such as nicotinamide back to NAD (Nikiforov et al., 2015). However, the synthetic pathways may not be important in the INH-mediated NAD accumulation in the liver, because (1) the synthesis of NAD may require a certain time to build up a high level of NAD and (2) NAD accumulation occurs sharply after INH treatment. Based on the role of NAD in redox reactions, protein deacetylation, and ADP-ribosylation (Pollak et al., 2007; Dolle et al., 2013), it is possible that overdose of INH inhibits the functions of the NAD-dependent enzymes. In addition, NAD can be hydrolyzed to ADP-ribose and nicotinamide in mitochondria by NAD-glycohydrolase (NADase) (Nakazawa et al., 1968; Zhang et al., 1995). We found that INH dose-dependently inhibits NADase activity (Figure 5C), suggesting that the INH-mediated accumulation of NAD is in part caused by INH-mediated NADase inhibition. Further studies are needed to determine the detailed mechanism by which overdose of INH leads to NAD accumulation in the liver.

Formation of INH-NAD adduct (VII)

Metabolite VII had a protonated molecule $[M+H]^+$ at m/z = 679 Da. MS/MS of metabolite VII produced the primary ions at m/z 542, 524, 428, and 136 (Figure 6A), which are exactly the same as the fragments of NAD (Figure 5A). However, the MW of metabolite VII is 15 Da larger

than NAD. We proposed the metabolite VII as an INH and NAD adduct in which the nicotinamide moiety in NAD was replaced by INH, because the MW difference of INH and nicotinamide is 15 Da. The structure of INH-NAD adduct was further confirmed by the studies using d4-INH (Figure 6B). In addition, the structure of the INH-NAD adduct reported in the current study was different from that of the previously reported INH-NAD adduct generated by the mycobacterial catalase-peroxidase enzyme KatG or host INH activation (Zhang et al., 1992; Mahapatra et al., 2012).

Formation of INH-NAD adduct is dose-dependent (Figure 6C). In the control group, no INH-NAD was detected. However, a considerable abundance of INH-NAD was detected in the liver of mice treated with 50 mg/Kg of INH, and it came to be much more abundant in the group treated with 200 mg/Kg (Figure 6C). We proposed that the formation of INH-NAD adduct is mediated by NADase. In addition to the activity of hydrolysis, NADase catalyzes the base-exchange reaction where it transfers the ADP-ribose moiety of NAD to pyridine derivatives such as nicotinamide and thionicotinamide (Nakazawa et al., 1968; Chini, 2009). INH contains a pyridine ring and its structure is similar to nicotinamide. Therefore, NADase may incorporate INH and ADP-ribose to form the INH-NAD adduct. We recaptured the formation of INH-NAD adduct using the purified NADase when it was co-incubated with equimolar amount of INH and NAD (Figure 6D). Further studies are needed to characterize the functions of INH-NAD adduct and its association with INH-induced liver damage.

INH-mediated accumulation of cystathionine (VIII)

Metabolite VIII was eluted at 0.81 min (Figure 7A). Metabolite VIII had a protonated molecule $[M+H]^+$ at *m/z* = 223 Da, with major fragments at *m/z* 134 and 88, which exactly matched to cystathionine (Figure 7B). The structure of cystathionine was further confirmed by comparing the retention time and MSMS to the authentic standard of cystathionine. INH-mediated accumulation of cystathionine is dose-dependent (Figure 7C).

Cystathionine is an important intermediate in the transsulfuration pathway (Stipanuk, 1986). Cystathionine beta synthase (CBS) and cystathionine gamma-lyase (CSE) are the enzymes for synthesizing and cleaving of cystathionine, respectively. Both CBS and CSE require the active form of vitamin B6 (pyridoxal phosphate, PLP) as a cofactor (Binkley et al., 1952). INH can cause vitamin B6 deficiency in part due to the formation of the INH and vitamin B6 adduct (Mandel, 1959). In the current study, an INH-PL adduct was detected in the serum of mice treated with INH (Figure 7D). In addition, the concentrations of PLP in the liver were dramatically decreased after INH treatment (Figure 7E). Although PLP is needed for both cystathionine synthesis and degradation, PLP deficiency affects CSE activity more than it affects CBS activity (Binkley et al., 1952; Hope, 1964). Therefore, we propose that accumulation of cystathionine in the liver after INH overdose is due to PLP deficiency (Figure 7F).

In the current study, we used an untargeted metabolomic approach to explore the INH-mediated global changes of endobiotic metabolites in mouse liver. We found that overdose of INH resulted in accumulation of oleoyl-L-carnitine and linoleoyl-L-carnitine in the liver, indicating mitochondrial dysfunction. We also revealed the interactions between INH and fatty acyl-CoAs by identifying INH-fatty acid amides. In addition, we found that overdose of INH led to the

accumulation of heme, NAD, and INH-NAD adduct in the liver. Furthermore, we illustrated that overdose of INH depleted vitamin B6 in the liver and blocked vitamin B6-dependent cystathionine degradation. All these hepatic biomarkers of INH presented in a dose-dependent manner, suggesting that a pharmacological dosage of INH can also interrupt the metabolism of endobiotics, especially for the slow metabolizers of N-acetyltransferase 2, in which INH metabolism is suppressed (Chen et al., 2006; Zabost et al., 2013). In summary, our data suggest that INH can disturb multiple endogenous pathways in the liver (Figure 8), which are potentially associated with INH-induced liver toxicity.

Authorship contributions

Participated in research design: Li, Wang, Ma

Conducted experiments: Li, Wang, Liu, Tarrago, Lu

Contributed the new reagents or analytic tools: Li, Wang, Liu, Tarrago, Chini

Performed data analysis: Li, Wang, Tarrago, Ma

Wrote or contributed to the writing of manuscript: Li, Wang, Ma

References

Bear ES, Hoffman PF, Siegel SR, and Randal RE, Jr. (1976) Suicidal ingestion of isoniazid: an uncommon cause of metabolic acidosis and seizures. *South Med J* **69:**31-32.

Beri R and Chandra R (1993) Chemistry and biology of heme. Effect of metal salts, organometals, and metalloporphyrins on heme synthesis and catabolism, with special reference to clinical implications and interactions with cytochrome P-450. *Drug Metab Rev* **25:**49-152.

Beyoglu D and Idle JR (2013) The metabolomic window into hepatobiliary disease. *J Hepatol* **59:**842-858.

Binkley F, Christensen GM, and Jensen WN (1952) Pyridoxine and the transfer of sulfur. *J Biol Chem* **194:**109-113.

Boelsterli UA and Lee KK (2014) Mechanisms of isoniazid-induced idiosyncratic liver injury – Emerging role of mitochondrial stress. *Journal of Gastroenterology and Hepatology***:**n/a-n/a.

Caksen H, Odabas D, Erol M, Anlar O, Tuncer O, and Atas B (2003) Do not overlook acute isoniazid poisoning in children with status epilepticus. *J Child Neurol* **18:**142-143.

Chen B, Li JH, Xu YM, Wang J, and Cao XM (2006) The influence of NAT2 genotypes on the plasma concentration of isoniazid and acetylisoniazid in Chinese pulmonary tuberculosis patients. *Clinica chimica acta; international journal of clinical chemistry* **365:**104-108.

Chen C, Krausz KW, Shah YM, Idle JR, and Gonzalez FJ (2009) Serum metabolomics reveals irreversible inhibition of fatty acid beta-oxidation through the suppression of PPARalpha activation as a contributing mechanism of acetaminophen-induced hepatotoxicity. *Chem Res Toxicol* **22:**699-707.

Cheng J, Krausz KW, Li F, Ma X, and Gonzalez FJ (2013) CYP2E1-dependent elevation of serum cholesterol, triglycerides, and hepatic bile acids by isoniazid. *Toxicol Appl Pharmacol* **266:**245-253.

Chini EN (2009) CD38 as a regulator of cellular NAD: a novel potential pharmacological target for metabolic conditions. *Current pharmaceutical design* **15:**57-63.

Church RJ, Wu H, Mosedale M, Sumner SJ, Pathmasiri W, Kurtz CL, Pletcher MT, Eaddy JS, Pandher K, Singer M, Batheja A, Watkins PB, Adkins K, and Harrill AH (2014) A systems biology approach utilizing a mouse diversity panel identifies genetic differences influencing isoniazid-induced microvesicular steatosis. *Toxicol Sci* **140:**481-492.

Dolle C, Rack JG, and Ziegler M (2013) NAD and ADP-ribose metabolism in mitochondria. *FEBS J* **280:**3530-3541.

Escande C, Nin V, Price NL, Capellini V, Gomes AP, Barbosa MT, O'Neil L, White TA, Sinclair DA, and Chini EN (2013) Flavonoid apigenin is an inhibitor of the NAD+ ase CD38: implications for cellular NAD+ metabolism, protein acetylation, and treatment of metabolic syndrome. *Diabetes* **62:**1084-1093.

Hope DB (1964) Cystathionine Accumulation in the Brains of Pyridoxine-Deficient Rats. *J Neurochem* **11:**327-332.

INCHEM (2016) Isoniazid. *http://wwwinchemorg/documents/pims/pharm/pim288htm*.

Khoharo HK, Ansari S, Abro A, and Qureshi F (2009) Suicidal Isoniazid poisoning. *J Ayub Med Coll Abbottabad* **21:**178-179.

Labbe G, Pessayre D, and Fromenty B (2008) Drug-induced liver injury through mitochondrial dysfunction: mechanisms and detection during preclinical safety studies. *Fundam Clin Pharmacol* **22:**335-353.

Lee KK, Fujimoto K, Zhang C, Schwall CT, Alder NN, Pinkert CA, Krueger W, Rasmussen T, and Boelsterli UA (2013) Isoniazid-induced cell death is precipitated by underlying mitochondrial complex I dysfunction in mouse hepatocytes. *Free Radic Biol Med* **65:**584-594.

Li F, Lu J, Cheng J, Wang L, Matsubara T, Csanaky IL, Klaassen CD, Gonzalez FJ, and Ma X (2013) Human PXR modulates hepatotoxicity associated with rifampicin and isoniazid co-therapy. *Nat Med* **19:**418-420.

Li F, Lu J, Wang L, and Ma X (2011a) CYP3A-mediated generation of aldehyde and hydrazine in atazanavir metabolism. *Drug metabolism and disposition: the biological fate of chemicals* **39:**394-401.

Li F, Miao Y, Zhang L, Neuenswander SA, Douglas JT, and Ma X (2011b) Metabolomic analysis reveals novel isoniazid metabolites and hydrazones in human urine. *Drug metabolism and pharmacokinetics* **26:**569-576.

Li F, Wang L, Guo GL, and Ma X (2010) Metabolism-mediated drug interactions associated with ritonavir-boosted tipranavir in mice. *Drug metabolism and disposition: the biological fate of chemicals* **38:**871-878.

Mahapatra S, Woolhiser LK, Lenaerts AJ, Johnson JL, Eisenach KD, Joloba ML, Boom WH, and Belisle JT (2012) A novel metabolite of antituberculosis therapy demonstrates host activation of isoniazid and formation of the isoniazid-NAD+ adduct. *Antimicrobial agents and chemotherapy* **56:**28-35.

Makowski L, Noland RC, Koves TR, Xing W, Ilkayeva OR, Muehlbauer MJ, Stevens RD, and Muoio DM (2009) Metabolic profiling of PPARalpha-/- mice reveals defects in carnitine

and amino acid homeostasis that are partially reversed by oral carnitine supplementation. *FASEB J* **23:**586-604.

Mandel W (1959) Pyridoxine and the isoniazid-induced neuropathy. *Diseases of the chest* **36:**293-296.

Maw G and Aitken P (2003) Isoniazid overdose : a case series, literature review and survey of antidote availability. *Clin Drug Investig* **23:**479-485.

McGill MR, Li F, Sharpe MR, Williams CD, Curry SC, Ma X, and Jaeschke H (2014) Circulating acylcarnitines as biomarkers of mitochondrial dysfunction after acetaminophen overdose in mice and humans. *Arch Toxicol* **88:**391-401.

Metushi IG, Nakagawa T, and Uetrecht J (2012) Direct oxidation and covalent binding of isoniazid to rodent liver and human hepatic microsomes: humans are more like mice than rats. *Chem Res Toxicol* **25:**2567-2576.

Nakazawa K, Ueda K, Honjo T, Yoshihara K, Nishizuka Y, and Hayaishi O (1968) Nicotinamide adenine dinucleotide glycohydrolases and poly adenosine diphosphate ribose synthesis in rat liver. *Biochem Biophys Res Commun* **32:**143-149.

Nikiforov A, Kulikova V, and Ziegler M (2015) The human NAD metabolome: Functions, metabolism and compartmentalization. *Critical reviews in biochemistry and molecular biology* **50:**284-297.

O'Connell TM and Watkins PB (2010) The application of metabonomics to predict drug-induced liver injury. *Clin Pharmacol Ther* **88:**394-399.

Olson KR, Kearney TE, Dyer JE, Benowitz NL, and Blanc PD (1993) Seizures associated with poisoning and drug overdose. *Am J Emerg Med* **11:**565-568.

Orcau A, Cayla JA, and Martinez JA (2011) Present epidemiology of tuberculosis. Prevention and control programs. *Enferm Infecc Microbiol Clin* **29 Suppl 1:**2-7.

Pessayre D, Fromenty B, Berson A, Robin MA, Letteron P, Moreau R, and Mansouri A (2012) Central role of mitochondria in drug-induced liver injury. *Drug Metab Rev* **44:**34-87.

Pessayre D, Mansouri A, Berson A, and Fromenty B (2010) Mitochondrial involvement in drug-induced liver injury. *Handb Exp Pharmacol***:**311-365.

Pollak N, Dolle C, and Ziegler M (2007) The power to reduce: pyridine nucleotides--small molecules with a multitude of functions. *Biochem J* **402:**205-218.

Ponka P (1999) Cell biology of heme. *Am J Med Sci* **318:**241-256.

Reagan-Shaw S, Nihal M, and Ahmad N (2008) Dose translation from animal to human studies revisited. *FASEB journal : official publication of the Federation of American Societies for Experimental Biology* **22:**659-661.

Richards VE, Chau B, White MR, and McQueen CA (2004) Hepatic gene expression and lipid homeostasis in C57BL/6 mice exposed to hydrazine or acetylhydrazine. *Toxicol Sci* **82:**318-332.

Romero JA and Kuczler FJ, Jr. (1998) Isoniazid overdose: recognition and management. *Am Fam Physician* **57:**749-752.

Ryter SW and Tyrrell RM (2000) The heme synthesis and degradation pathways: role in oxidant sensitivity. Heme oxygenase has both pro- and antioxidant properties. *Free Radic Biol Med* **28:**289-309.

Sampey BP, Freemerman AJ, Zhang J, Kuan PF, Galanko JA, O'Connell TM, Ilkayeva OR, Muehlbauer MJ, Stevens RD, Newgard CB, Brauer HA, Troester MA, and Makowski L

(2012) Metabolomic profiling reveals mitochondrial-derived lipid biomarkers that drive obesity-associated inflammation. *PLoS One* **7:**e38812.

Shuhendler AJ, Pu K, Cui L, Uetrecht JP, and Rao J (2014) Real-time imaging of oxidative and nitrosative stress in the liver of live animals for drug-toxicity testing. *Nat Biotechnol* **32:**373-380.

Stipanuk MH (1986) Metabolism of sulfur-containing amino acids. *Annual review of nutrition* **6:**179-209.

Tai DY, Yeo JK, Eng PC, and Wang YT (1996) Intentional overdosage with isoniazid: case report and review of literature. *Singapore Med J* **37:**222-225.

Temmerman W, Dhondt A, and Vandewoude K (1999) Acute isoniazid intoxication: seizures, acidosis and coma. *Acta Clin Belg* **54:**211-216.

Tenhunen R, Marver HS, and Schmid R (1968) The enzymatic conversion of heme to bilirubin by microsomal heme oxygenase. *Proc Natl Acad Sci U S A* **61:**748-755.

Tenhunen R, Marver HS, and Schmid R (1969) Microsomal heme oxygenase. Characterization of the enzyme. *J Biol Chem* **244:**6388-6394.

van der Ham M, Albersen M, de Koning TJ, Visser G, Middendorp A, Bosma M, Verhoeven-Duif NM, and de Sain-van der Velden MG (2012) Quantification of vitamin B6 vitamers in human cerebrospinal fluid by ultra performance liquid chromatography-tandem mass spectrometry. *Anal Chim Acta* **712:**108-114.

Wagener FA, Eggert A, Boerman OC, Oyen WJ, Verhofstad A, Abraham NG, Adema G, van Kooyk Y, de Witte T, and Figdor CG (2001) Heme is a potent inducer of inflammation in mice and is counteracted by heme oxygenase. *Blood* **98:**1802-1811.

Wagener FA, Volk HD, Willis D, Abraham NG, Soares MP, Adema GJ, and Figdor CG (2003) Different faces of the heme-heme oxygenase system in inflammation. *Pharmacol Rev* **55:**551-571.

WHO (2013) Global tuberculosis report. *http://wwwwhoint/tb/publications/global_report/en/*.

Zabost A, Brzezinska S, Kozinska M, Blachnio M, Jagodzinski J, Zwolska Z, and Augustynowicz-Kopec E (2013) Correlation of N-acetyltransferase 2 genotype with isoniazid acetylation in Polish tuberculosis patients. *BioMed research international* **2013:**853602.

Zhang J, Ziegler M, Schneider R, Klocker H, Auer B, and Schweiger M (1995) Identification and purification of a bovine liver mitochondrial NAD(+)-glycohydrolase. *FEBS Lett* **377:**530-534.

Zhang Y, Heym B, Allen B, Young D, and Cole S (1992) The catalase-peroxidase gene and isoniazid resistance of Mycobacterium tuberculosis. *Nature* **358:**591-593.

Footnotes

This work was supported in part by the National Institute of Diabetes and Digestive and Kidney Diseases [Grant number DK090305]. The authors declare that there are no conflicts of interest.

F.L. and P.W. contributed equally to this work.

Figure legends

Figure 1. Metabolomic analysis of mouse liver from the control and INH-treated groups. WT mice were treated with vehicle or 200 mg/Kg INH (*p.o.*). Liver samples were collected 30 min after treatment. All samples were analyzed by UPLC-QTOFMS. (A) Separation of control and INH-treated groups in a PCA score plot. The t[1] and t[2] values represent the score of each sample in principal component 1 and 2, respectively. (B) Loading S-plot generated by OPLS-DA analysis. The *X*-axis is a measure of the relative abundance of ions and the *Y*-axis is a measure of the correlation of each ion to the model.

Figure 2. Accumulation of heme (I) in the liver of mice treated with INH. A, the extracted chromatogram of heme. B, MS/MS of heme. C, relative abundance of heme. The data are expressed as mean ± SEM (n = 3). ***$p < 0.001$ vs control group.

Figure 3. Accumulation of oleoyl-L-carnitine (II) and linoleoyl-L-carnitine (III) in the liver of mice treated with INH. A, extracted chromatograms of acylcarnitines II and III. B, MS/MS of oleoyl-L-carnitine (II). C, MS/MS of linoleoyl-L-carnitine (III). D, relative abundance of acylcarnitines II and III in the liver. The data are expressed as mean ± SEM (n = 3). **$p < 0.01$, ***$p < 0.001$ vs control group.

Figure 4. Formation of INH-fatty acid amides (IV and V). A, extracted chromatograms of amides IV and V. B, MS/MS of amide IV. C, MS/MS of amide V. D, relative abundance of amides IV and V. The data are expressed as mean ± SEM (n = 3). **$p < 0.01$ vs control group. E, the scheme of the formation of INH-fatty acid amides. N.D., not detected.

Figure 5. Accumulation of NAD (VI) in the liver of mice treated with INH. A, MS/MS of NAD. B, relative abundance of NAD in the liver. The data are expressed as mean ± SEM (n = 3). ***$p < 0.001$ vs control group. C, the inhibitory effect of INH on NADase activity.

Figure 6. Formation of INH-NAD adduct (VII) in the liver of mice treated with INH. A, MS/MS of INH-NAD adduct. B, MS/MS of d4-INH-NAD adduct. C, relative abundance of INH-NAD adduct in the liver. D, the role of NADase in the formation of INH-NAD adduct. N.D., not detected. The quantified data are expressed as mean ± SEM (n = 3). *$p < 0.001$ vs control group.

Figure 7. Accumulation of cystathionine (VIII) in the liver of mice treated with INH. A, the extracted chromatogram of cystathionine from the liver. B, MS/MS of cystathionine. C, relative abundance of cystathionine in the liver. D, MS/MS of INH-PL adduct. E, relative abundance of PLP in the liver. All quantified data are expressed as mean ± SEM (n = 3). **$p < 0.01$, ***$p < 0.001$ vs control group. F, the proposed mechanism by which INH disturbs cystathionine homeostasis. CSE, cystathionine gamma-lyase; PLP, pyridoxal phosphate.

Figure 8. The scheme of disturbance of endogenous pathways in mouse liver by a high dose of INH. FA, fatty acid.

Fig. 1

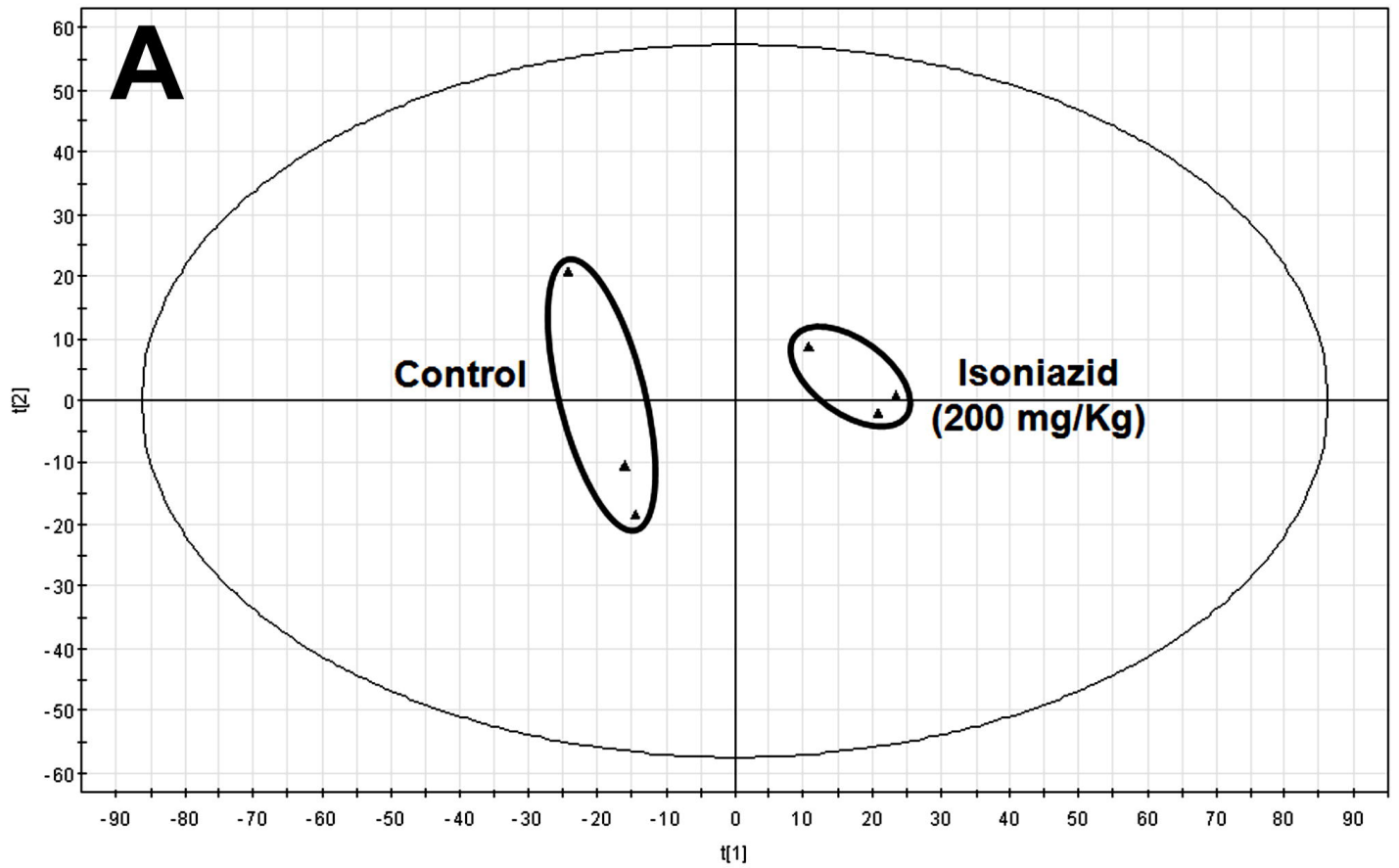
A
Control
Isoniazid
(200 mg/Kg)
t[2]
t[1]

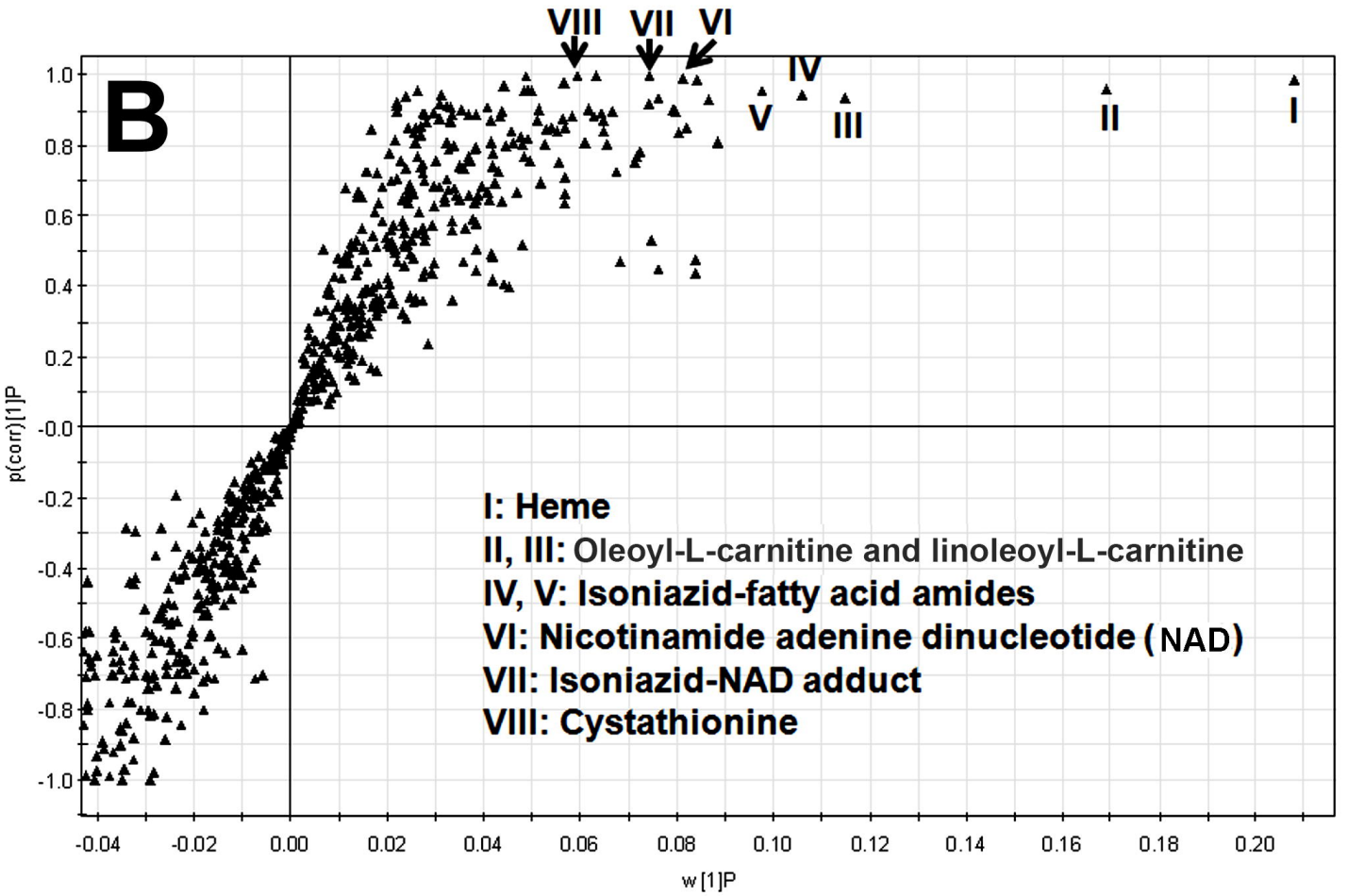
B
VIII
VII
VI
IV
V
III
II
I
p(corr)[1]P
w[1]P
I: Heme
II, III: Oleoyl-L-carnitine and linoleoyl-L-carnitine
IV, V: Isoniazid-fatty acid amides
VI: Nicotinamide adenine dinucleotide (NAD)
VII: Isoniazid-NAD adduct
VIII: Cystathionine

Fig. 2

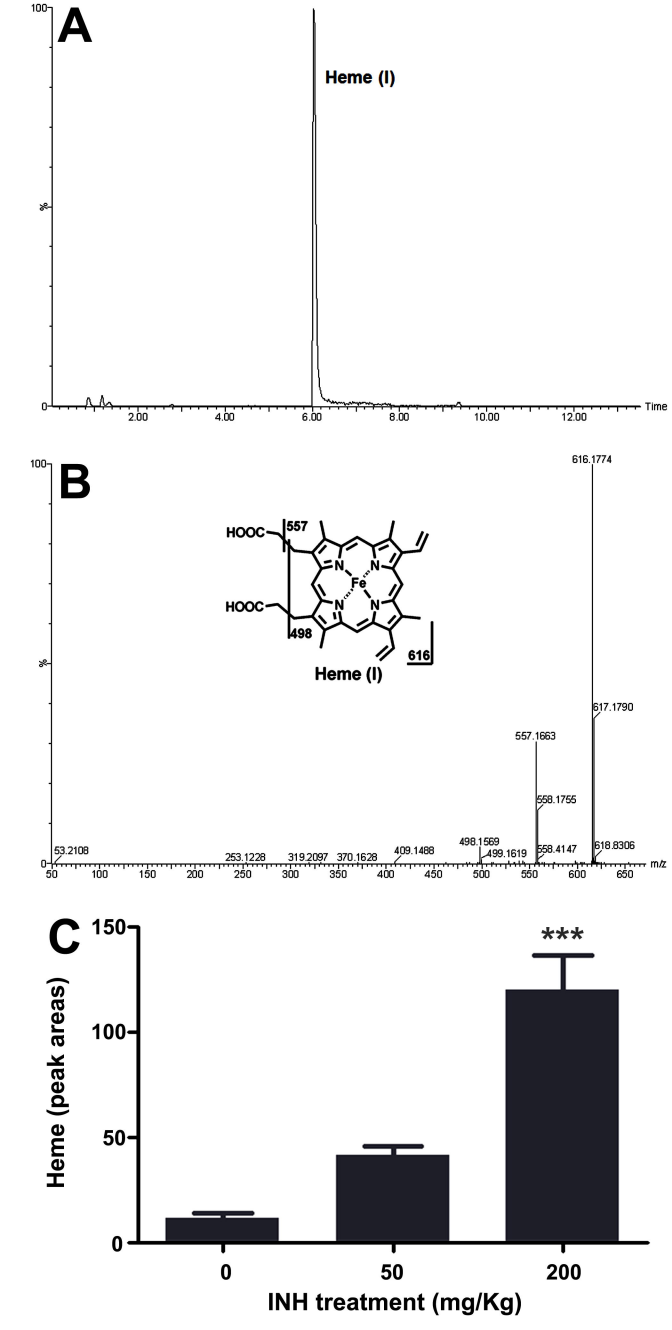
A
Heme (I)
100
%
0
2.00
4.00
6.00
8.00
10.00
12.00
Time
B
100
%
0
HOOC
557
HOOC
498
Fe
N
N
N
N
616
Heme (I)
616.1774
617.1790
557.1663
558.1755
618.8306
558.4147
499.1619
498.1569
409.1488
370.1628
319.2097
253.1228
53.2108
50
100
150
200
250
300
350
400
450
500
550
600
650
m/z
C
150
100
50
0
Heme (peak areas)
***
0
50
200
INH treatment (mg/Kg)

Fig. 3

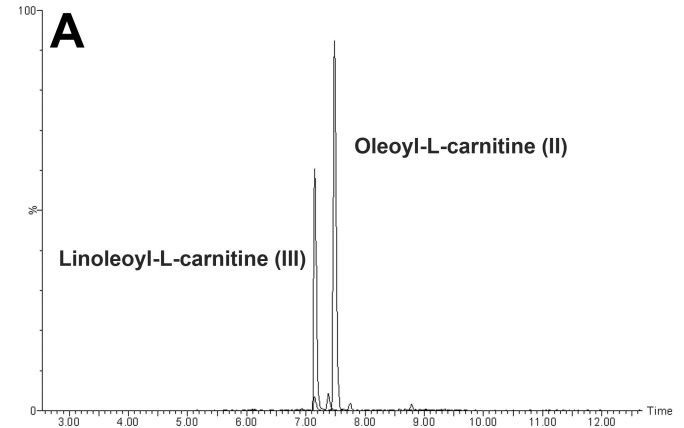
A
Oleoyl-L-carnitine (II)
Linoleoyl-L-carnitine (III)
%
Time
3.00
4.00
5.00
6.00
7.00
8.00
9.00
10.00
11.00
12.00

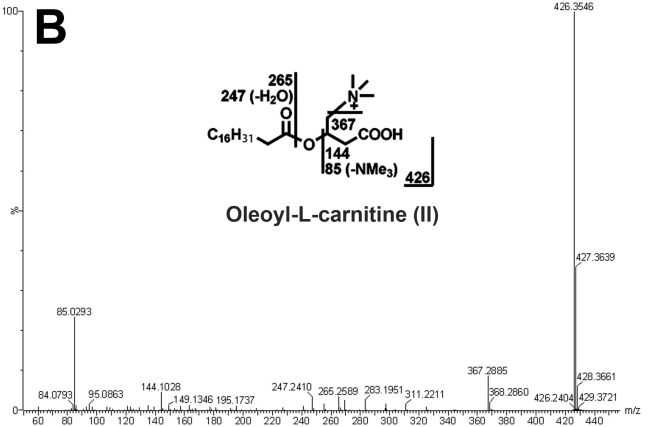
B
426.3546
265
247 (-H2O)
C16H31
367
COOH
144
85 (-NMe3)
426
Oleoyl-L-carnitine (II)
427.3639
85.0293
367.2885
428.3661
84.0793
95.0863
144.1028
149.1346
195.1737
247.2410
265.2589
283.1951
311.2211
368.2860
426.2404
429.3721
m/z

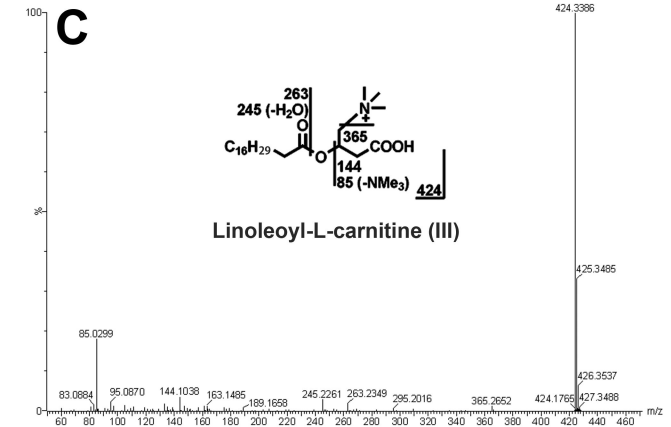
C
424.3386
263
245 (-H2O)
C16H29
365
COOH
144
85 (-NMe3)
424
Linoleoyl-L-carnitine (III)
425.3485
85.0299
426.3537
83.0864
95.0870
144.1038
163.1485
189.1658
245.2261
263.2349
295.2016
365.2652
424.1765
427.3488
m/z

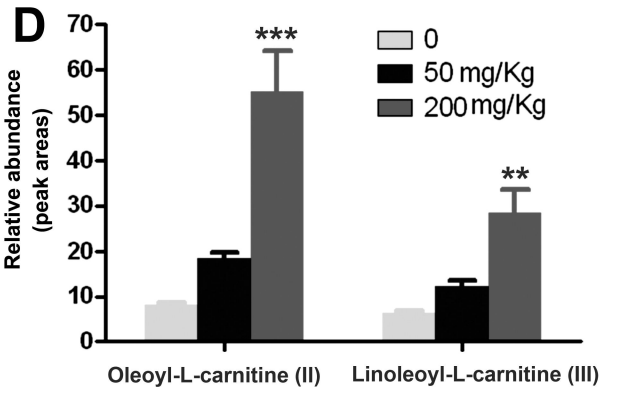
D
Relative abundance
(peak areas)
0
50 mg/Kg
200 mg/Kg
***
**
Oleoyl-L-carnitine (II)
Linoleoyl-L-carnitine (III)

Fig. 4

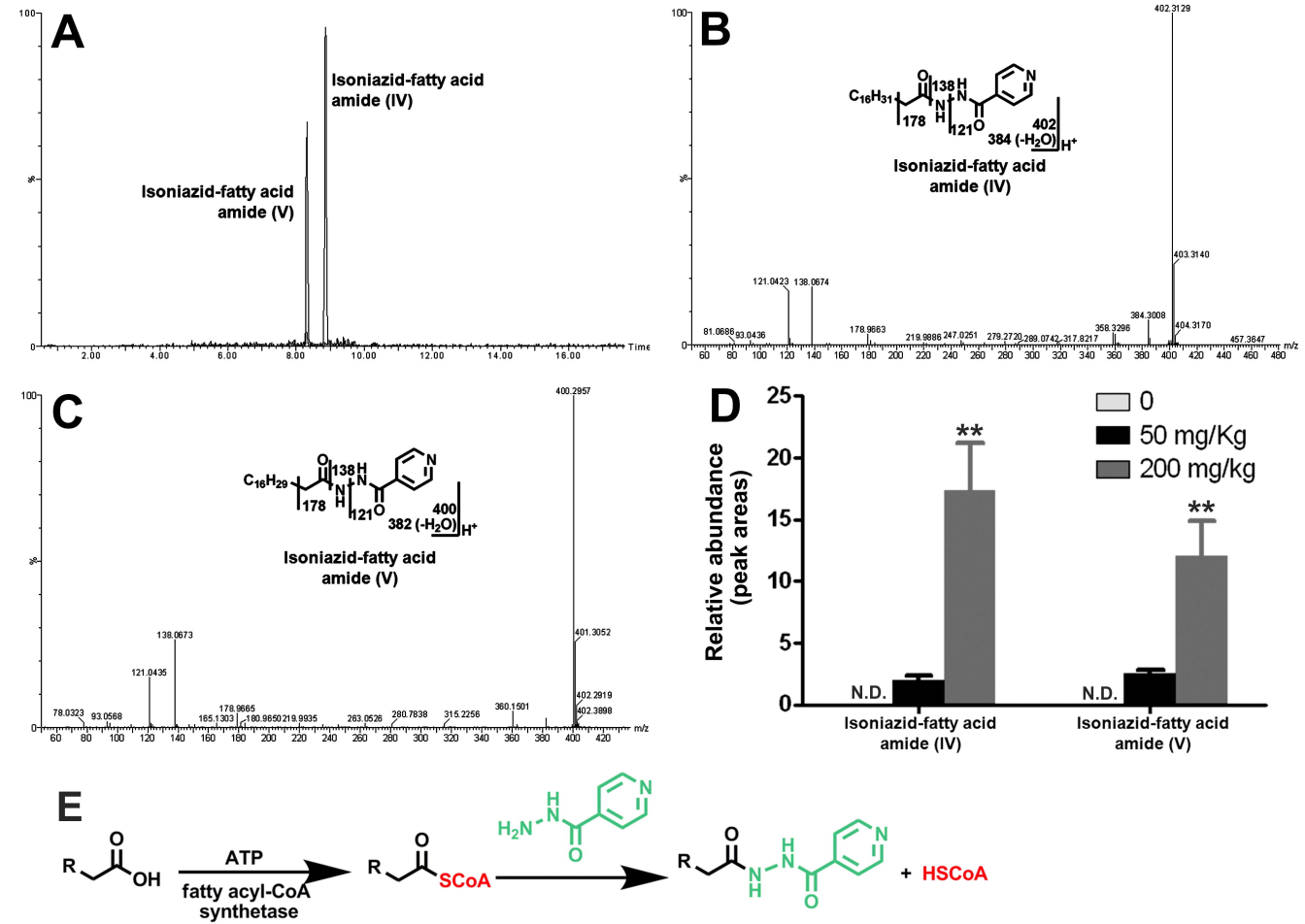
A
Isoniazid-fatty acid amide (IV)
Isoniazid-fatty acid amide (V)
B
Isoniazid-fatty acid amide (IV)
C
Isoniazid-fatty acid amide (V)
D
Relative abundance (peak areas)
0
50 mg/Kg
200 mg/kg
N.D.
Isoniazid-fatty acid amide (IV)
Isoniazid-fatty acid amide (V)
E
ATP
fatty acyl-CoA synthetase
SCoA
+ HSCoA

Fig. 5

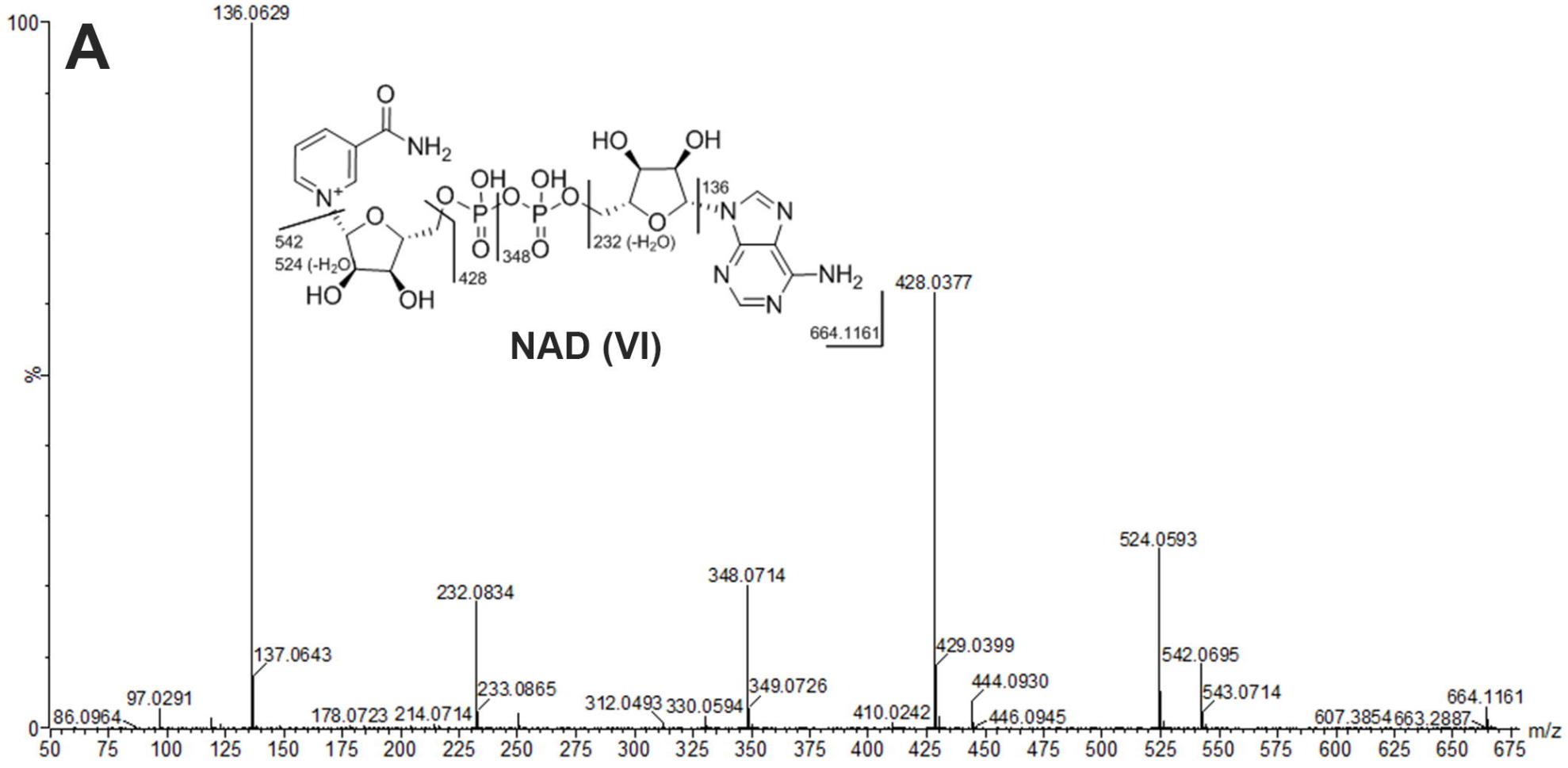
A
NAD (VI)
136.0629
428.0377
664.1161
524.0593
348.0714
232.0834
137.0643
429.0399
542.0695
444.0930
543.0714
233.0865
349.0726
97.0291
86.0964
178.0723
214.0714
312.0493
330.0594
410.0242
446.0945
607.3854
663.2887
664.1161
%
m/z
542
524 (-H2O)
428
348
232 (-H2O)
136

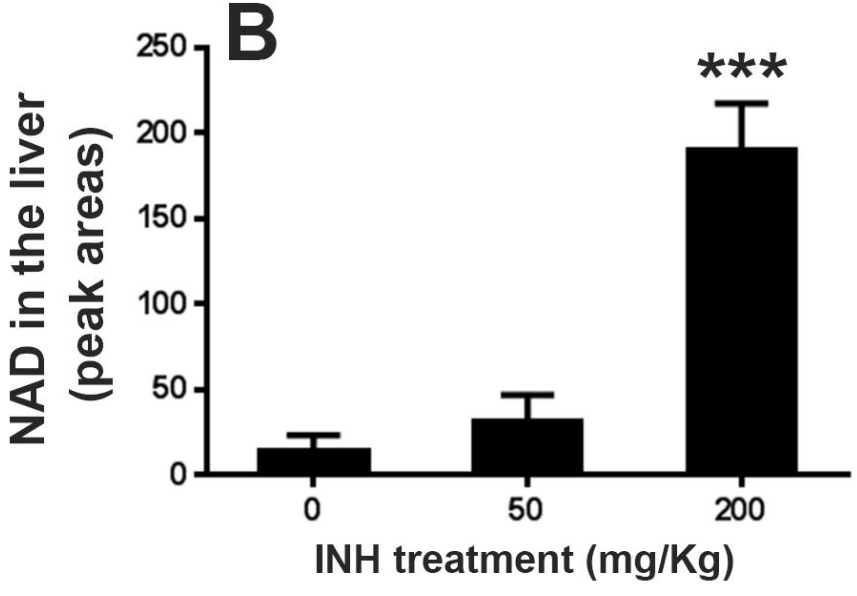
B
***
NAD in the liver
(peak areas)
INH treatment (mg/Kg)
0
50
200

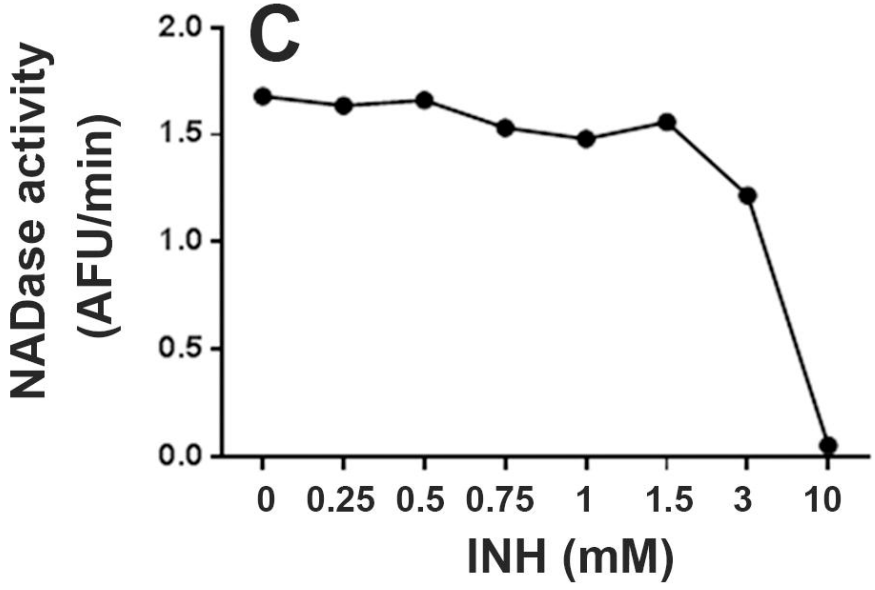
C
NADase activity
(AFU/min)
INH (mM)
0
0.25
0.5
0.75
1
1.5
3
10

Fig. 6

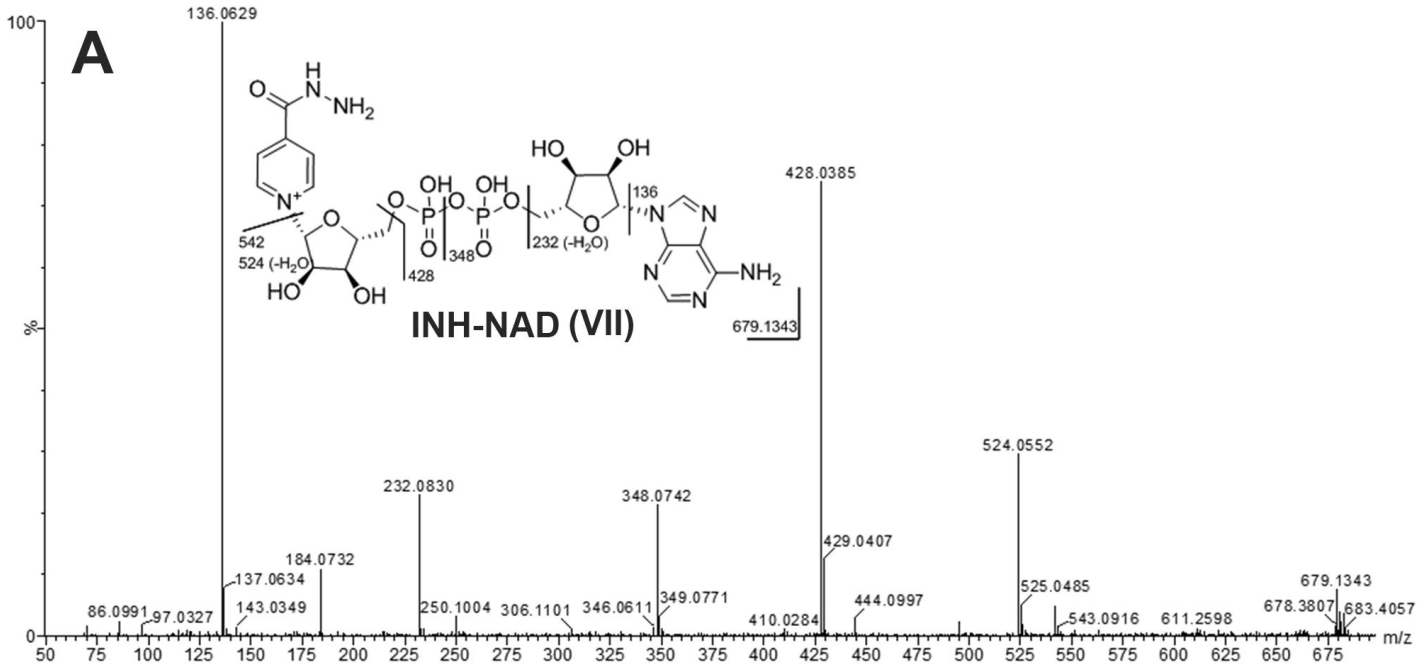
A
INH-NAD (VII)
136.0629
428.0385
524.0552
232.0830
348.0742
429.0407
184.0732
137.0634
525.0485
679.1343
86.0991
97.0327
143.0349
250.1004
306.1101
346.0611
349.0771
410.0284
444.0997
543.0916
611.2598
678.3807
683.4057
679.1343
m/z

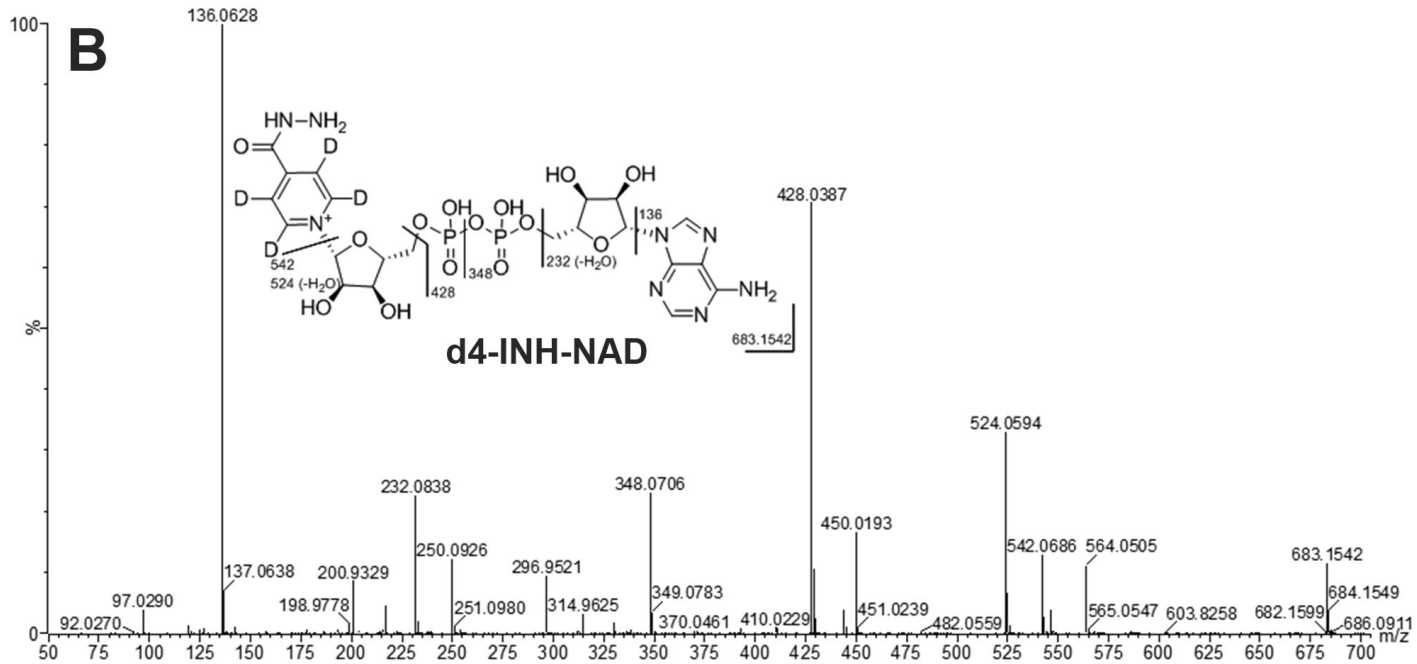
B
d4-INH-NAD
136.0628
428.0387
524.0594
232.0838
348.0706
450.0193
250.0926
542.0686
564.0505
683.1542
137.0638
200.9329
296.9521
97.0290
198.9778
349.0783
684.1549
92.0270
251.0980
314.9625
370.0461
410.0229
451.0239
482.0559
565.0547
603.8258
682.1599
686.0911
m/z

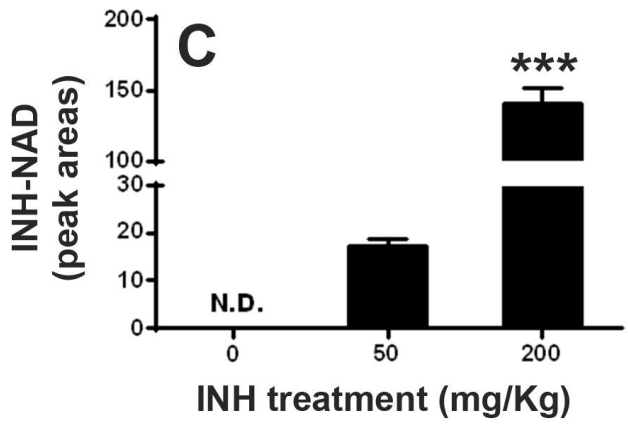
C
INH-NAD (peak areas)
***
N.D.
0
50
200
INH treatment (mg/Kg)

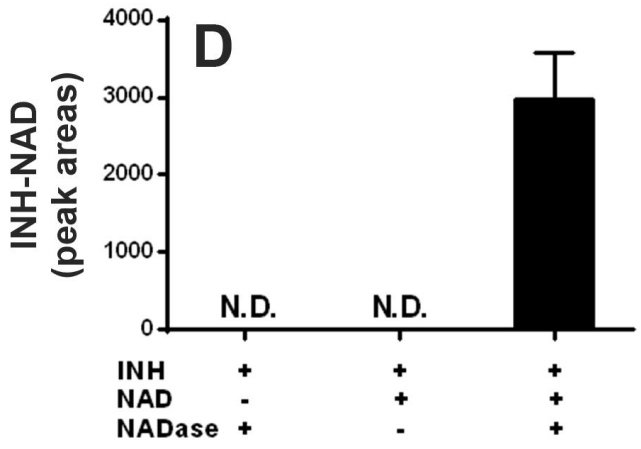
D
INH-NAD (peak areas)
N.D.
N.D.
INH + + +
NAD - + +
NADase + - +

Fig. 7

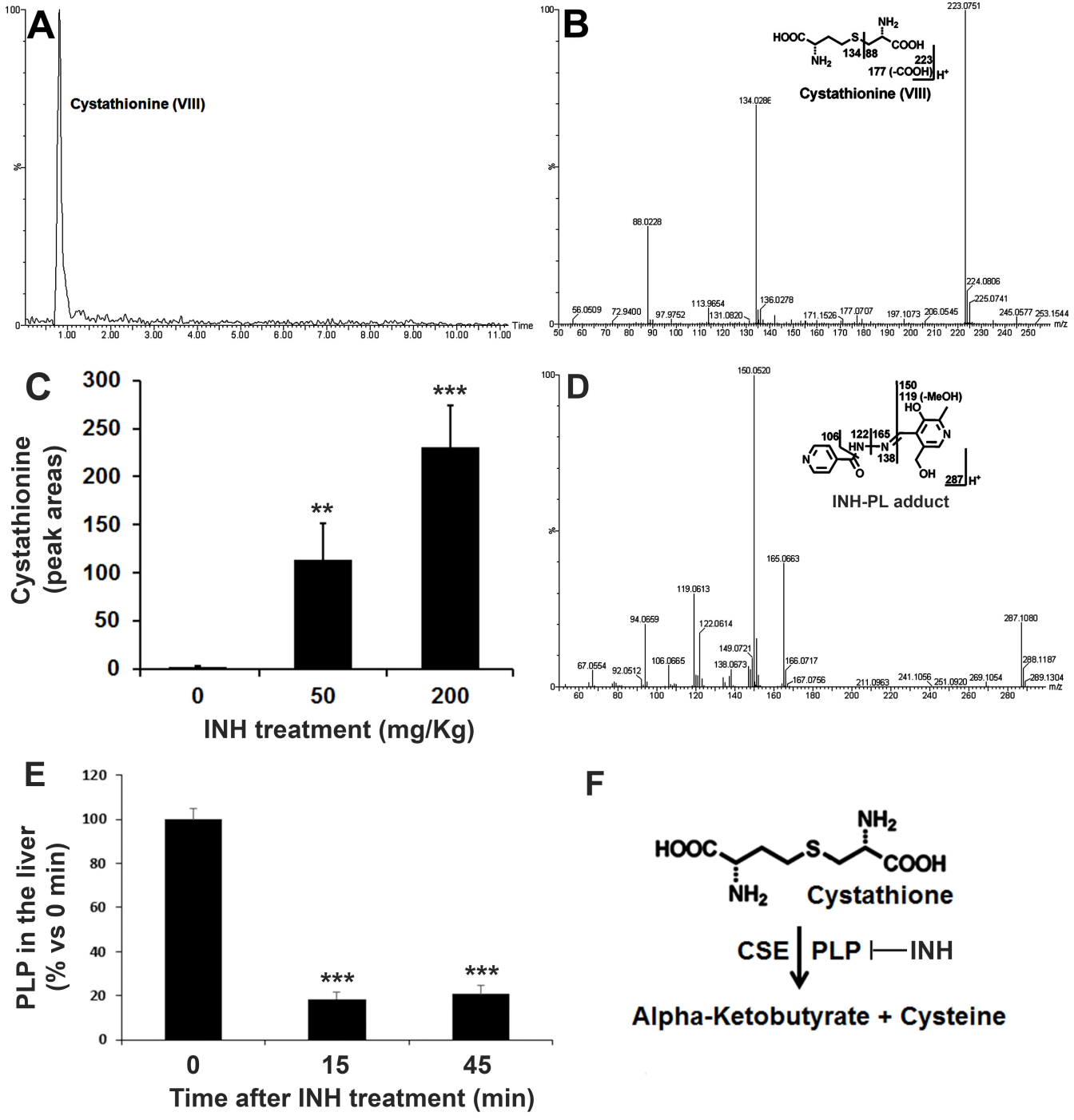
A
Cystathionine (VIII)
Time
B
Cystathionine (VIII)
C
Cystathionine (peak areas)
INH treatment (mg/Kg)
0
50
200
**
***
D
INH-PL adduct
E
PLP in the liver (% vs 0 min)
Time after INH treatment (min)
0
15
45
***
***
F
Cystathione
CSE
PLP
INH
Alpha-Ketobutyrate + Cysteine

Fig. 8

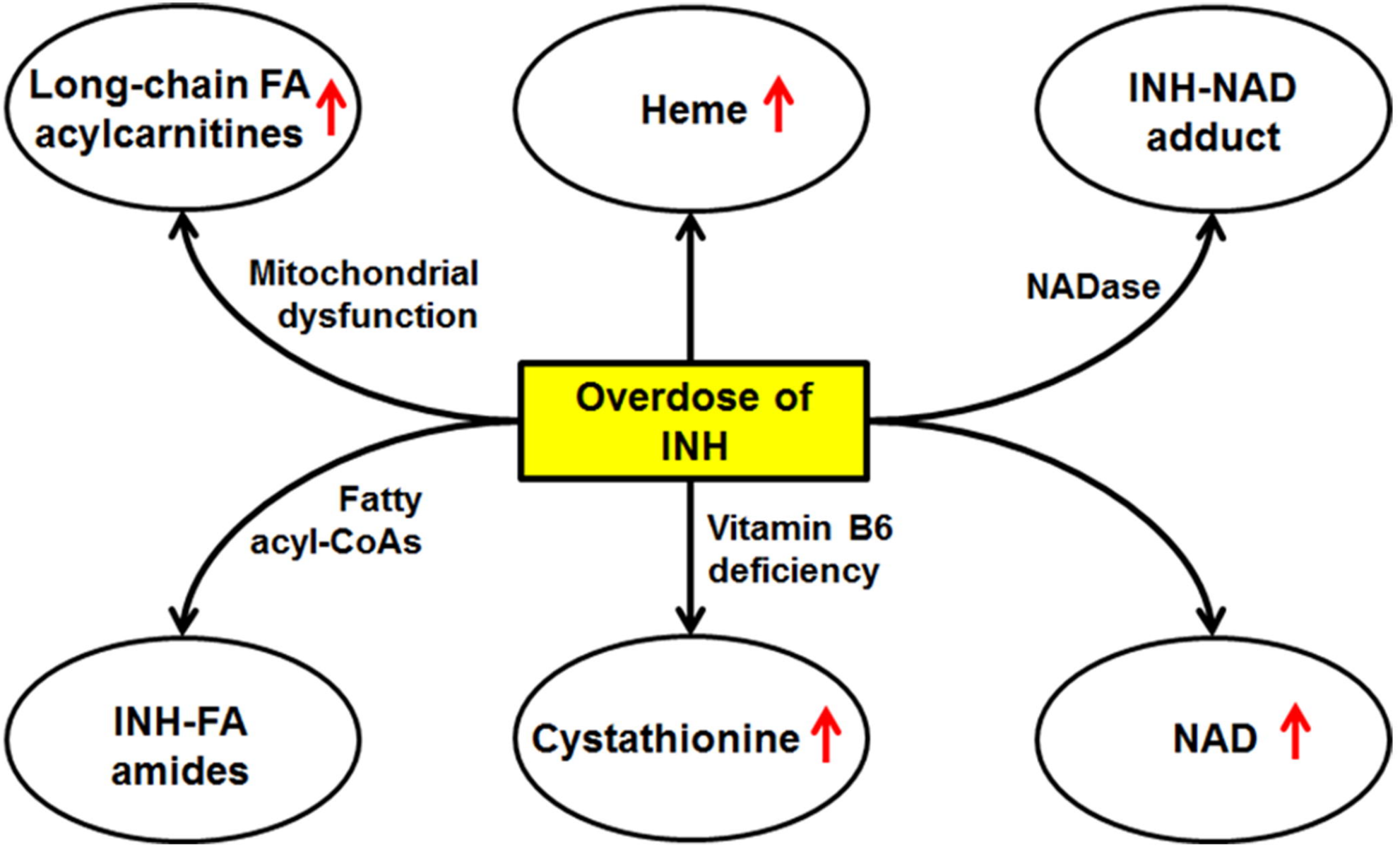
Long-chain FA acylcarnitines
Heme
INH-NAD adduct
Mitochondrial dysfunction
NADase
Overdose of INH
Fatty acyl-CoAs
Vitamin B6 deficiency
INH-FA amides
Cystathionine
NAD